IEEE Photonics Journal
An IEEE Photonics Society Publication

Two-Step Phase-Shifting Algorithm Based on the Quadratic Spatial Filtering of Interferograms

Volume 12, Number 6, December 2020

Xianxin Han
Linna Xie
Yi Wang
Jiaosheng Li
Liyun Zhong
Xiaoxu Lu

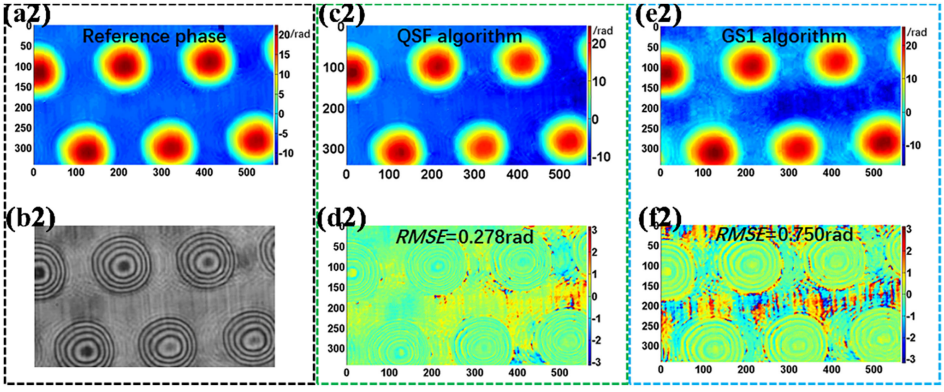

DOI: 10.1109/JPHOT.2020.3033299

Two-Step Phase-Shifting Algorithm Based on the Quadratic Spatial Filtering of Interferograms

Xianxin Han, Linna Xie, Yi Wang, Jiaosheng Li, Liyun Zhong, and Xiaoxu Lu

Guangdong Provincial Key Laboratory of Nanophotonic Functional Materials and Devices, South China Normal University, Guangzhou 510006, China

DOI:10.1109/JPHOT.2020.3033299

Manuscript received September 28, 2020; accepted October 19, 2020. Date of publication October 23, 2020; date of current version December 9, 2020. This work was supported in part by the National Natural Science Foundation of China under Grants 61727814, 61875059 and 61805086, and in part by the Science and Technology Program of Guangzhou under Grant 2019050001. Corresponding author: Xiaoxu Lu (e-mail: hsgdzlxx@scnu.edu.cn).

Abstract: By using the quadratic spatial filtering (QSF) operation of interferograms, we propose a fast and accurate phase retrieval algorithm in 2-step phase-shifting interferometry (PSI), in which both the interference signal separation and blind phase shift estimation can be realized. Compared with the existed 2-step PSI algorithms, the proposed QSF algorithm reveals two advantages: First, when the background intensity is not accurately estimated, which is a serious problem in 2-step PSI, the distortion of the retrieved phase can be released. Second, there is no requirement about the fringe density of interference pattern, reflecting the phase shift estimation can be realized even if the fringes density is sparse. The former is a valuable solution to reduce most significant errors in 2-step PSI, and the latter makes the accuracy robust against different fringe patterns. Both the simulation and experimental results demonstrate the excellent performance of the proposed QSF algorithm.

Index Terms: Interferometry, fringe analysis, phase measurement.

1. Introduction

Phase-Shifting interferometry (PSI), a full-field and quantitative phase measurement technology, has been used in various fields [1], [2] over the past decades. Compared with other phase measurement methods [3]–[6], by encoding the phase signal into interferogram in a linear way, PSI offers a deterministic and accurate solution for phase retrieval. Moreover, by introducing the phase shift between interferograms for signal demodulation, PSI can be realized in temporal domain [7], [8], spatial domain [9], [10], or their hybrid [11], [12]. In addition, as a computational imaging technology, different phase coding strategies in PSI will reveal different advantages and disadvantages. Temporal PSI can fully use the space-bandwidth product of image detector while the spatial PSI can realize single-shot measurement. In temporal PSI, the requirement of many phase shift interferograms makes it sensitive to the environmental vibration [13], [14], and the accuracy of self-calibration algorithm plays an important role in accurate phase retrieval due to the uncertainty of phase shift [15]–[19]. Recently, although some good solutions are proposed, the accuracy of self-calibration algorithm is greatly related to the fringe's number. For instance, in order

to remove the error induced by the additional aberration removal procedure, the phase aberration is physically compensated [8], [20], so only the phase induced by the sample can generate fringes and total fringes' number will become small. In this case, many algorithms will encounter accuracy decreasing or even cannot work. Actually, the spatial PSI is a spatial-multiplexing technology, in which the phase coding and decoding way is similar with Fourier transform phase demodulation method [21]–[23], so only less than one-third of total spatial-bandwidth product of camera can be used in conventional spatial PSI due to the inevitable band-pass filtering operation.

2-step PSI is first proposed in [24] and then causes more and more attention [25]–[34], in which only 2-frame interferograms are enough for phase retrieval while at least 3-frame interferograms are necessary in conventional PSI, therefore both temporal and spatial information can be fully used. Consequently, high temporal resolution and vibrational robustness can be expected. Since only one-time phase shift is necessary, so 2-step PSI is a good solution for dynamic phase measurement. Compared with the spatial multiplexing methods, which can obtain 2-frame interferograms simultaneously [35]–[38], 2-step PSI can reserve more high frequency component of the encoded phase corresponding to the details of the measured sample.

Although with significant advantage as a compromise solution of temporal and spatial PSI, 2-step PSI has a challenge: The background intensity removal operation, which is usually realized by the temporal subtraction in temporal PSI [39] or the spatial filtering [21] in spatial PSI and the high-pass filtering operation [40] used in 2-frame interferograms will lead to serious phase distortion, especially near the location with sparse fringes [17]. To address this, a lot of algorithms are proposed to remove the background [41]–[43] and it is assumed that the background intensity is a slowly changed signal relative to the interference intensity, which is not usually valid in practice. Another task in 2-step PSI is to blindly estimate the phase shift. Generally speaking, the accuracy of phase shift estimation is also strongly related to the fringe's number in the interferograms.

In this study, we propose a new 2-step PSI algorithm based on the quadratic spatial filtering (QSF) of interferograms, in which the phase distortion induced by the background-removal operation can be released by properly using a direct subtracted-interferogram. What's more, the blind phase shift estimation is not related to the fringe number, and the accuracy of phase retrieval is robust against different fringe patterns. Following, we will introduce the details of the proposed QSF algorithm.

2. Principle and Analysis

2.1 Basic Procedure of the Quadratic Spatial Filtering (QSF) Algorithm

In general, 2-frame interferograms in 2-step PSI can be described as:

$$I_1(\boldsymbol{r}) = A(x,y) + B(x,y)\cos\phi(x,y) = A(\boldsymbol{r}) + B(\boldsymbol{r})\cos\phi(\boldsymbol{r}) \tag{1a}$$

$$I_2(\boldsymbol{r}) = A(x,y) + B(x,y)\cos[\phi(x,y)+\delta] = A(\boldsymbol{r}) + B(\boldsymbol{r})\cos[\phi(\boldsymbol{r})+\delta] \tag{1b}$$

Here, $\boldsymbol{r} = (x, y)$ denotes 2-dimension coordinate; $A(\boldsymbol{r})$ and $B(\boldsymbol{r})$ represent the background intensity and the modulation amplitude, respectively; the phase shift between two interferograms is δ. Usually, in conventional 2-step PSI, the background intensity $A(\boldsymbol{r})$ is filtered in advance, we have that:

$$\begin{aligned} P_1(\boldsymbol{r}) &= \mathcal{F}^{-1}\{H(\boldsymbol{f})\mathcal{F}[I_1(\boldsymbol{r}) + I_2(\boldsymbol{r})]\} \\ &= \mathcal{F}^{-1}\left[H(\boldsymbol{f})\mathcal{F}\left\{2A(\boldsymbol{r}) + 2B(\boldsymbol{r})\cos\left(\frac{\delta}{2}\right)\cos\left[\phi(\boldsymbol{r}) + \frac{\delta}{2}\right]\right\}\right] \\ &\approx 2B(\boldsymbol{r})\cos\left(\frac{\delta}{2}\right)\cos\left[\phi(\boldsymbol{r}) + \frac{\delta}{2}\right] \end{aligned} \tag{2a}$$

$$P_2(\boldsymbol{r}) = I_1(\boldsymbol{r}) - I_2(\boldsymbol{r}) = 2B(\boldsymbol{r})\sin\left(\frac{\delta}{2}\right)\sin\left[\phi(\boldsymbol{r}) + \frac{\delta}{2}\right] \tag{2b}$$

Here, $\mathcal{F}$ and $\boldsymbol{f}$ represent the Fourier transform operation and spatial frequency, respectively; $H(\boldsymbol{f})$ denotes a high-pass filter. The aim of direct subtraction between two interferograms (Eq. (2b)) is expected to save time and release the phase distortion induced by the filtering bank. If δ is known, $B(x)\cos\phi(x)$ and $B(x)\sin\phi(x)$ can be determined by solving linear equations Eqs. (2a) and (2b). In order to estimate δ, it is needed to make some reasonable assumptions. As we know, in conventional 2-step PSI, the background removal procedure is based on the fact that $A(\boldsymbol{r})$ is a slowly varying function while the property of $B(\boldsymbol{r})$ has not been considered. In principle, $B(\boldsymbol{r})$ can also be assumed as a slowly varying function, we can obtain more information. However, because $B(\boldsymbol{r})$ is multiplied with the cosine/sine terms of phase $\phi(\boldsymbol{r})$, its utilization is not easy. To address this, in this study, we implement a quadratic procedure for $P_1(\boldsymbol{r})$ and $P_2(\boldsymbol{r})$:

$$T_1(\boldsymbol{r}) = P_1(\boldsymbol{r})^2 \approx 2B(\boldsymbol{r})^2\cos^2\left(\frac{\delta}{2}\right)\{1+\cos[2\phi(\boldsymbol{r})+\delta]\} \tag{3a}$$

$$T_2(\boldsymbol{r}) = P_2(\boldsymbol{r})^2 = 2B^2(\boldsymbol{r})\sin^2\left(\frac{\delta}{2}\right)\{1-\cos[2\phi(\boldsymbol{r})+\delta]\} \tag{3b}$$

Subsequently, by performing the similar procedure in Eq. (2a), we can remove the DC components in Eqs. (3a) and (3b) by high-pass spatial filtering as following:

$$\tilde{T}_1(\boldsymbol{r}) = \mathcal{F}^{-1}\{H(\boldsymbol{f})\mathcal{F}[T_1(\boldsymbol{r})]\} \approx 2B(\boldsymbol{r})^2\cos^2\left(\frac{\delta}{2}\right)\cos[2\phi(\boldsymbol{r})+\delta] \tag{4a}$$

$$\tilde{T}_2(\boldsymbol{r}) = \mathcal{F}^{-1}\left\{H(\boldsymbol{f})\mathcal{F}[T_2(\boldsymbol{r})]\right\} \approx -2B^2(\boldsymbol{r})\sin^2\left(\frac{\delta}{2}\right)\cos[2\phi(\boldsymbol{r})+\delta] \tag{4b}$$

Where $\tilde{T}(\boldsymbol{r})$ denotes the high-pass filtering result of $T(\boldsymbol{r})$. Clearly, in Eqs. (4a) and (4b), the same cosine terms are modulated. That is to say, there is a constant c that can satisfy following equation:

$$\tilde{T}_2(\boldsymbol{r}) + c\tilde{T}_1(\boldsymbol{r}) \approx 0 \tag{5}$$

In order to determine the value of c, we define a cost function as:

$$K(c) = \sum\sum_{\boldsymbol{r}}\left[\tilde{T}_2 + c\tilde{T}_1(\boldsymbol{r})\right]^2 \tag{6}$$

Thus, the value of c can be determined by solving a linear least-square equation. If Eq. (5) can be satisfied, we have that:

$$T_2(\boldsymbol{r}) + cT_1(\boldsymbol{r}) = L_0(\boldsymbol{r}) \propto B^2(\boldsymbol{r}) \tag{7a}$$

$$[P_2(\boldsymbol{r})]^2 + \left[\sqrt{c}P_1(\boldsymbol{r})\right]^2 = L_0(\boldsymbol{r}) \propto B^2(\boldsymbol{r}) \tag{7b}$$

Here, $L_0(\boldsymbol{r})$ is a quasi-constant in spatial domain which is proportional to $B^2(\boldsymbol{r})$ because from $T_1(\boldsymbol{r})$, $T_2(\boldsymbol{r})$ to $\tilde{T}_1(\boldsymbol{r})$, $\tilde{T}_2(\boldsymbol{r})$, the removed DC term is proportional to $B^2(\boldsymbol{r})$. Clearly, $P_1(\boldsymbol{r})$ and $P_2(\boldsymbol{r})$ are two linear combinations of $B(\boldsymbol{r})\cos\phi(\boldsymbol{r})$ and $B(\boldsymbol{r})\sin\phi(\boldsymbol{r})$ as shown in Eqs. (2a) and (2b), so we have that:

$$J_1(\boldsymbol{r}) = P_2(\boldsymbol{r}) = mB(\boldsymbol{r})\cos\left[\phi(\boldsymbol{r})+\delta'\right] \tag{8a}$$

$$J_2(\boldsymbol{r}) = \sqrt{c}P_1(\boldsymbol{r}) = mB(\boldsymbol{r})\sin\left[\phi(\boldsymbol{r})+\delta'\right] \tag{8b}$$

Here, δ' is an unessential piston term which can be neglected and m is a trivial constant. Then, $\phi(\boldsymbol{r})$ can be calculated by:

$$\phi(\boldsymbol{r}) = \arg[J_1(\boldsymbol{r}) + iJ_2(\boldsymbol{r})] \tag{9}$$

Note that two important approximations are respectively introduced in Eq. (2a), Eqs. (4a) and (4b), and these equations can be strictly satisfied only when Fourier spatial filtering can accurately estimate and remove the DC-terms, i.e., $A(\boldsymbol{r})$ and $B^2(\boldsymbol{r})$. Actually, in most cases, especially when the fringe's number is not large enough, the above approximations cannot be satisfied, the distortion

will appear in the retrieved phase. In this study, we implement 3-time spatial filtering operations instead of 2-time in most other algorithms [25]–[34]. However, in the obtained interference signals i.e., $J_1(\boldsymbol{r})$ and $J_2(\boldsymbol{r})$ in our QSF algorithm, only $J_1(\boldsymbol{r})$ is implemented spatial filtering, so the accuracy should be improved, and the detailed analysis is presented in section 2.2. Note that the second and third FFT operations in the QSF algorithm are used in Eqs. (4a) and (4b) for c value estimation. The utilization of FFT and high pass filtering is to remove $B^2(\boldsymbol{r})$ instead regarding it as a constant, like the strategy in ellipse fitting technology, the former is suitable for the non-uniformity of illumination.

2.2 The Distortion Analysis for 2-Step PSI

In this section, we will discuss how the distortion of the retrieved phase is introduced in the spatial filtering operation, and then implement a quantitative characterization about this distortion. First, we consider an interference term by the filtering operation. If the size of interferogram is set as $S_x \times S_y$, we have that:

$$\begin{aligned} h(\boldsymbol{r}) \otimes B(\boldsymbol{r}) \cos[\phi(\boldsymbol{r}) + \delta] &= \sum \sum_{\tau_x=1,\tau_y=1}^{\tau_x=S_x,\tau_y=S_y} h(\boldsymbol{\tau}) B(\boldsymbol{r}-\boldsymbol{\tau}) \cos[\phi(\boldsymbol{r}-\boldsymbol{\tau}) + \delta] \\ &= \sum \sum_{\tau_x=1,\tau_y=1}^{\tau_x=S_x,\tau_y=S_y} h(\boldsymbol{\tau}) B(\boldsymbol{r}-\boldsymbol{\tau}) \cos[\phi(\boldsymbol{r}) + f(\boldsymbol{r},\boldsymbol{\tau}) + \delta] \\ &= \cos[\phi(\boldsymbol{r}) + \delta] \sum \sum_{\tau_x=1,\tau_y=1}^{\tau_x=S_x,\tau_y=S_y} h(\boldsymbol{\tau}) B(\boldsymbol{r}-\boldsymbol{\tau}) \cos[f(\boldsymbol{r},\boldsymbol{\tau})] \\ &\quad - \sin[\phi(\boldsymbol{r}) + \delta] \sum \sum_{\tau_x=1,\tau_y=1}^{\tau_x=S_x,\tau_y=S_y} h(\boldsymbol{\tau}) B(\boldsymbol{r}-\boldsymbol{\tau}) \sin[f(\boldsymbol{r},\boldsymbol{\tau})] \\ &= \sqrt{T(\boldsymbol{r})} \cos[\phi(\boldsymbol{r}) + \delta + \eta(\boldsymbol{r})] = \sqrt{T(\boldsymbol{r})} \cos\left[\phi'(\boldsymbol{r}) + \delta\right] \end{aligned} \tag{10}$$

Where $\otimes$ denotes the spatial convolution, and the functions $f(\boldsymbol{r},\boldsymbol{\tau})$, $T(\boldsymbol{r})$, $\eta(\boldsymbol{r})$, $\phi'(\boldsymbol{r})$ are defined as:

$$f(\boldsymbol{r},\boldsymbol{\tau}) = \phi(\boldsymbol{r}-\boldsymbol{\tau}) - \phi(\boldsymbol{r}) \tag{11a}$$

$$T(\boldsymbol{r}) = \left[\sum \sum_{\tau_x=1,\tau_y=1}^{\tau_x=S_x,\tau_y=S_y} h(\boldsymbol{\tau}) B(\boldsymbol{r}-\boldsymbol{\tau}) \sin[f(\boldsymbol{r},\boldsymbol{\tau})]\right]^2 + \left[\sum \sum_{\tau_x=1,\tau_y=1}^{\tau_x=S_x,\tau_y=S_y} h(\boldsymbol{\tau}) B(\boldsymbol{r}-\boldsymbol{\tau}) \cos[f(\boldsymbol{r},\boldsymbol{\tau})]\right]^2 \tag{11b}$$

$$\eta(\boldsymbol{r}) = \arccos\left[\frac{\sum \sum_{\tau_x=1,\tau_y=1}^{\tau_x=S_x,\tau_y=S_y} h(\boldsymbol{\tau}) B(\boldsymbol{r}-\boldsymbol{\tau}) \cos[f(\boldsymbol{r},\boldsymbol{\tau})]}{\sqrt{T(\boldsymbol{r})}}\right] \tag{11c}$$

$$\phi'(\boldsymbol{r}) = \phi(\boldsymbol{r}) + \eta(\boldsymbol{r}) \tag{11d}$$

From Eqs. (11a)–(11d), we can see that in the interference term, the encoded phase distribution is changed from $\phi(\boldsymbol{r})$ to $\phi'(\boldsymbol{r})$ and the modulation amplitude is changed from $B(\boldsymbol{r})$ to $\sqrt{T(\boldsymbol{r})}$ after the spatial filtering operation. And from Eq. (10), it is found that the phase distortion appears in the spatial domain, but the phase shift remains unchanged after the spatial filtering operation. Clearly, this result will provide a guarantee of c value estimation from Eqs. (4) and (5).

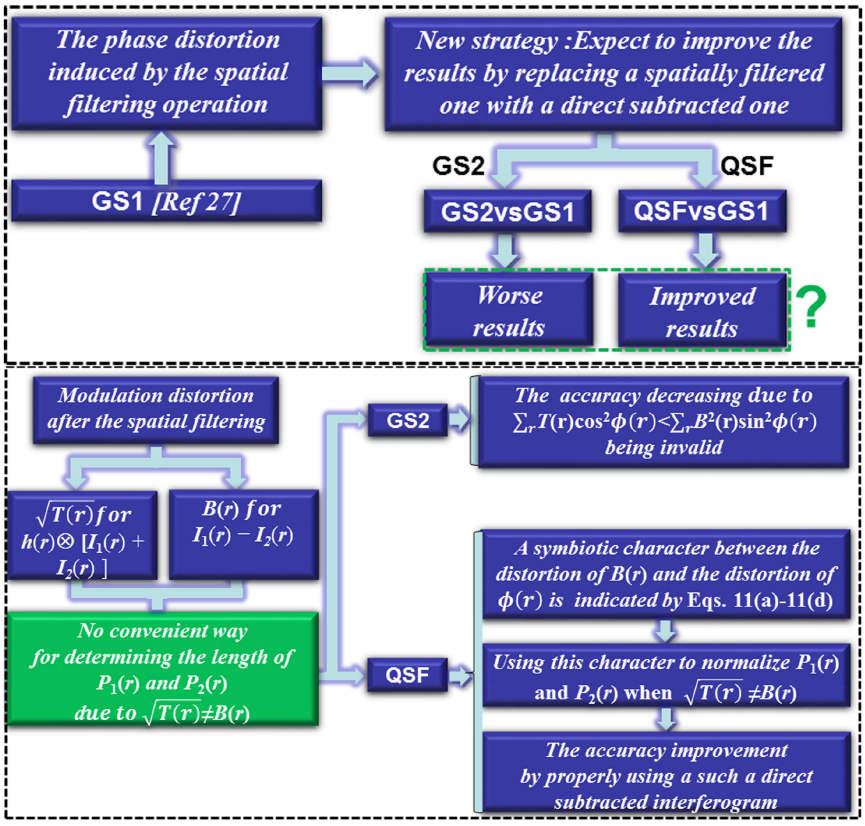

Fig. 1. The flow chart of releasing phase distortion with the proposed QSF algorithm.

What's more, Eqs. (11a)-(11d) present a symbiotic character between the modulation amplitude distortion ($B(\boldsymbol{r})$ to $\sqrt{T(\boldsymbol{r})}$) and the phase distortion ($\phi(\boldsymbol{r})$ to $\phi'(\boldsymbol{r})$) by the spatial filtering. That is to say, the more serious phase distortion exists, the more serious modulation amplitude distortion appears. Intuitively, if the spatial filtering operation introduces the distortion in the retrieved phase, by replacing a spatial filtered-interferogram with a direct subtracted-interferogram (Eq. (2b)), we can realize the accuracy improvement of phase retrieval. At the first glance, it seems that all 2-step PSI methods are benefit from the similar strategy. Actually, this improvement can be realized only when the information of modulation amplitude is properly used for 2-step phase retrieval. For comparison, we present the result of GS algorithm [27], in which a spatial filtered-interferogram is replaced with a direct subtracted-interferogram. It is found that the accuracy is not improved as expected but deteriorated instead. Next, we will explain the reason that the QSF algorithm release the phase distortion by properly using the direct subtracted-interferogram. For ease of understanding, Fig. 1 gives a flow chart to present the reason and procedure of releasing phase distortion with the proposed QSF algorithm.

In the conventional strategy, based on the spatial filtering, 2-frame background-removed interferograms can be described as:

$$\tilde{I}_1(\boldsymbol{r}) = \sqrt{T(\boldsymbol{r})}\cos[\phi(\boldsymbol{r})+\eta(\boldsymbol{r})] \tag{12a}$$

$$\tilde{I}_2(\boldsymbol{r}) = \sqrt{T(\boldsymbol{r})}\cos[\phi(\boldsymbol{r})+\eta(\boldsymbol{r})+\delta] = \sqrt{T(\boldsymbol{r})}\cos[\phi(\boldsymbol{r})+\eta(\boldsymbol{r})]\cos(\delta) - \sqrt{T(\boldsymbol{r})}\sin[\phi(\boldsymbol{r})+\eta(\boldsymbol{r})]\sin(\delta) \tag{12b}$$

In Eqs. (11a)-(11d), $\eta(\boldsymbol{r})$ represents the additional phase term reflecting the phase distortion and $\sqrt{T(\boldsymbol{r})}$ represents the distorted modulation amplitude. In order to obtain $\sqrt{T(\boldsymbol{r})}\sin[\phi(\boldsymbol{r})+\eta(\boldsymbol{r})]$ from

$\tilde{I}_1(\boldsymbol{r})$ and $\tilde{I}_2(\boldsymbol{r})$, we have that:

$$\sqrt{T(\boldsymbol{r})}\sin[\phi(\boldsymbol{r})+\eta(\boldsymbol{r})]=\frac{\tilde{I}_2(\boldsymbol{r})}{\sin(\delta)}-\cot(\delta)\cdot\tilde{I}_1(\boldsymbol{r})=k_1\tilde{I}_2(\boldsymbol{r})-k_2\tilde{I}_1(\boldsymbol{r}) \tag{13a}$$

$$k_1=\frac{1}{\sin(\delta)},k_2=\cot(\delta) \tag{13b}$$

In this case, we can obtain accurate k_1 and k_2 because even both the phase and modulation are distorted, the following relationship [27] is still valid:

$$\sum\sum_{\tau_x=1,\tau_y=1}^{\tau_x=S_x,\tau_y=S_y}T(\boldsymbol{r})\cos^2\left[\phi'(\boldsymbol{r})\right]\ll\sum\sum_{\tau_x=1,\tau_y=1}^{\tau_x=S_x,\tau_y=S_y}T(\boldsymbol{r})\sin\left[\phi'(\boldsymbol{r})\right]\cos\left[\phi'(\boldsymbol{r})\right] \tag{14a}$$

$$\sum\sum_{\tau_x=1,\tau_y=1}^{\tau_x=S_x,\tau_y=S_y}T(\boldsymbol{r})\cos^2\left[\phi'(\boldsymbol{r})\right]\approx\sum\sum_{\tau_x=1,\tau_y=1}^{\tau_x=S_x,\tau_y=S_y}T(\boldsymbol{r})\sin^2\left[\phi'(\boldsymbol{r})\right] \tag{14b}$$

However, after introducing the direct subtracted-interferogram and considering the distortion, Eqs. (2a) and (2b) can be rewritten as:

$$\begin{aligned}P_1(\boldsymbol{r})&=\mathcal{F}^{-1}\{H(\boldsymbol{f}_r)\mathcal{F}[I_1(\boldsymbol{r})+I_2(\boldsymbol{r})]\}\\&=\mathcal{F}^{-1}\left[H(\boldsymbol{f}_r)\mathcal{F}\left\{2A(\boldsymbol{r})+2B(\boldsymbol{r})\cos\left(\frac{\delta}{2}\right)\cos[\phi(\boldsymbol{r})+\delta]\right\}\right]\\&\approx 2\sqrt{T(\boldsymbol{r})}\cos\left(\frac{\delta}{2}\right)\cos\left[\phi(\boldsymbol{r})+\frac{\delta}{2}\right]\end{aligned} \tag{15a}$$

$$P_2(\boldsymbol{r})=I_1(\boldsymbol{r})-I_2(\boldsymbol{r})=2B(\boldsymbol{r})\sin\left(\frac{\delta}{2}\right)\sin\left[\phi(\boldsymbol{r})+\frac{\delta}{2}\right] \tag{15b}$$

Note that the modulation amplitude in $P_1(\boldsymbol{r})$ is different from $P_2(\boldsymbol{r})$, i.e., $\sqrt{T(\boldsymbol{r})}$ and $B(\boldsymbol{r})$. Due to the loss of low-frequency spatial filtering, there is the expression $\sqrt{T(\boldsymbol{r})}<B(\boldsymbol{r})$ according to Parseval's theorem. In this case, we cannot properly normalize$P_1(\boldsymbol{r})$ and $P_2(\boldsymbol{r})$ due to:

$$\sum\sum_{\tau_x=1,\tau_y=1}^{\tau_x=S_x,\tau_y=S_y}T(\boldsymbol{r})\cos^2\left[\phi'(\boldsymbol{r})\right]<\sum\sum_{\tau_x=1,\tau_y=1}^{\tau_x=S_x,\tau_y=S_y}T(\boldsymbol{r})\sin^2\left[\phi'(\boldsymbol{r})\right] \tag{16}$$

Thus, the assumption of GS algorithm will become invalid.

On the contrary, the QSF algorithm provides a convenient solution for the normalization of $P_1(\boldsymbol{r})$ and $P_2(\boldsymbol{r})$. As mentioned in Eqs. (10)-(11) that the distortion of $\phi(\boldsymbol{r})$ is accompanied with the distortion of $B(\boldsymbol{r})$. Meanwhile, the distortion of $B(\boldsymbol{r})$ is reflected as the fringe's intensity, by changing it from a slowly varying function to a rapidly varying function, the spatial high-frequency component will increase. That is to say, in QSF algorithm, by compensating high-frequency component in the obtained modulation amplitude according to Eqs. (4-7), we can normalize$P_1(\boldsymbol{r})$ and $P_2(\boldsymbol{r})$ in a suitable way. As a result, this directly subtracted interferogram can be properly used, and the accuracy of phase retrieval can be improved.

3. Numerical Evaluation

In order to verify the above theoretical analysis, we use 2-frame simulated fringe patterns to perform phase retrieval with three different algorithms, i.e., GS algorithm with 2-frame spatial filtered-interferograms $\tilde{I}_1(\boldsymbol{r})$, $\tilde{I}_2(\boldsymbol{r})$ named as GS1, GS algorithm with 1-frame direct subtracted-interferogram and 1-frame spatial filtered-interferogram $\tilde{I}_1(\boldsymbol{r})$, $I_1(\boldsymbol{r})-I_2(\boldsymbol{r})$ named as GS2 and the proposed QSF algorithm with $\tilde{I}_1(\boldsymbol{r})+\tilde{I}_2(\boldsymbol{r})$, $I_1(\boldsymbol{r})-I_2(\boldsymbol{r})$.

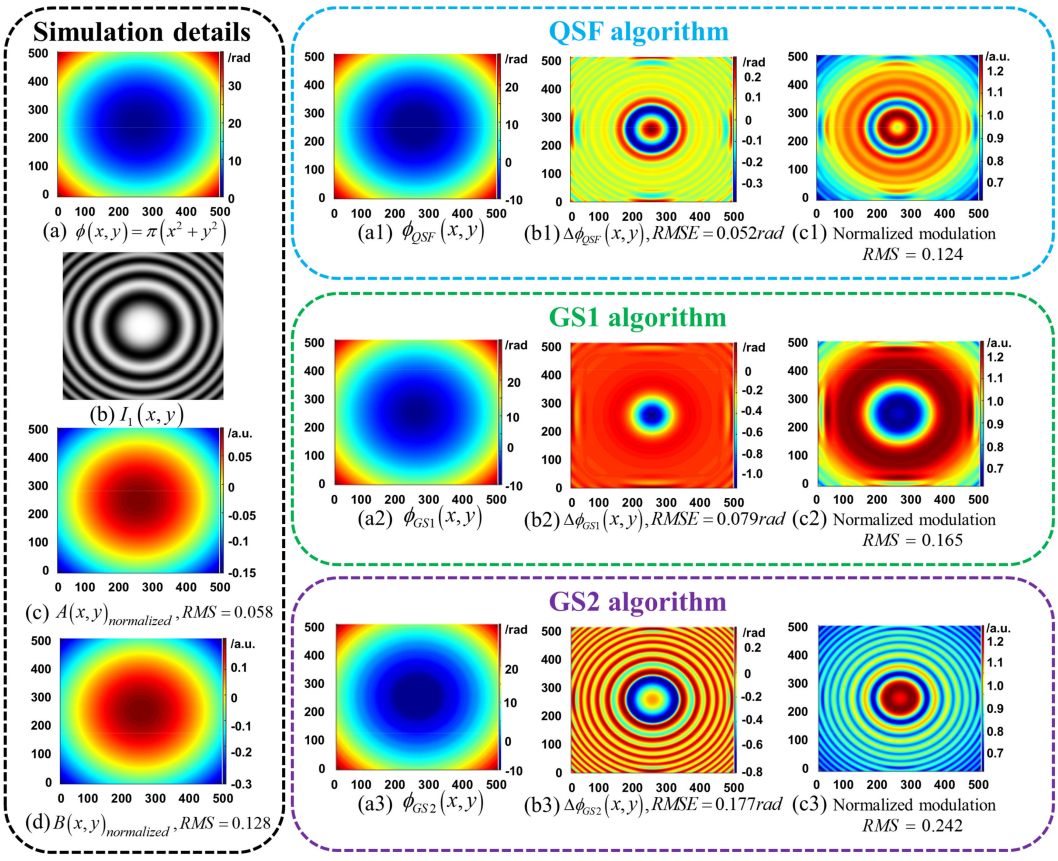

Fig. 2. (a)–(d) simulation details; (a1)–(a3) the phase distribution obtained by the QSF, GS1 and GS2 algorithm, respectively; (b1)–(b3) the phase errors between (a) and (a1-a3), respectively; (c1)–(c3) the normalized modulation amplitudes obtained by the QSF, GS1 and GS2 algorithm, respectively, in which root mean square (*RMS)* is used to describe the spatially changing rate of a given function.

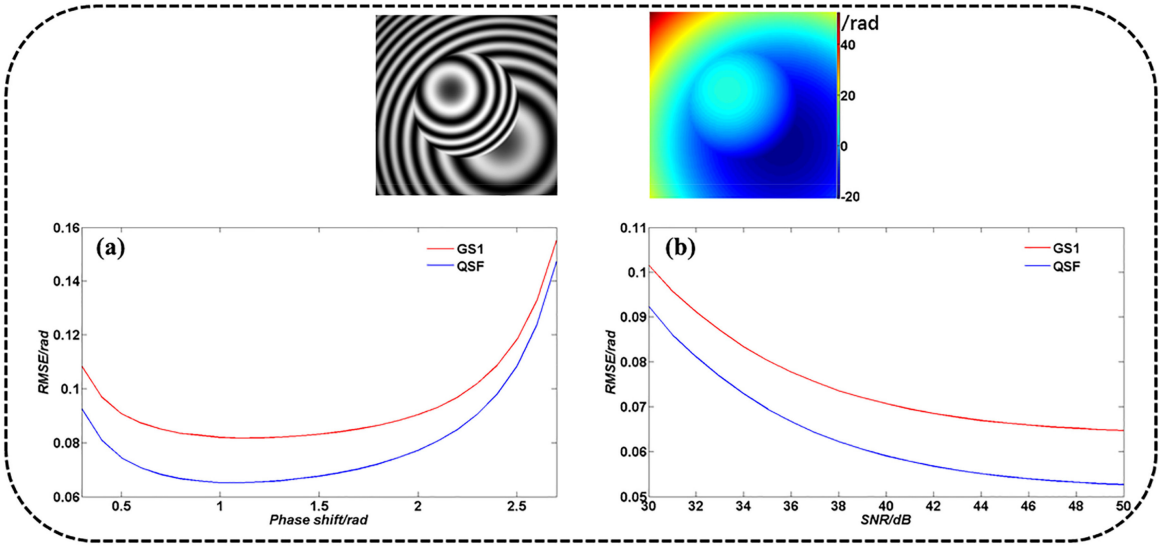

Fig. 3. The variations of RMSEs with different (a) phase shifts; (b) SNRs of interference patterns, in which $A(x, y) = 50exp[-0.1(x^2 + y^2)] + 50$, $B(x, y) = 50exp[-0.1(x^2 + y^2)]$.

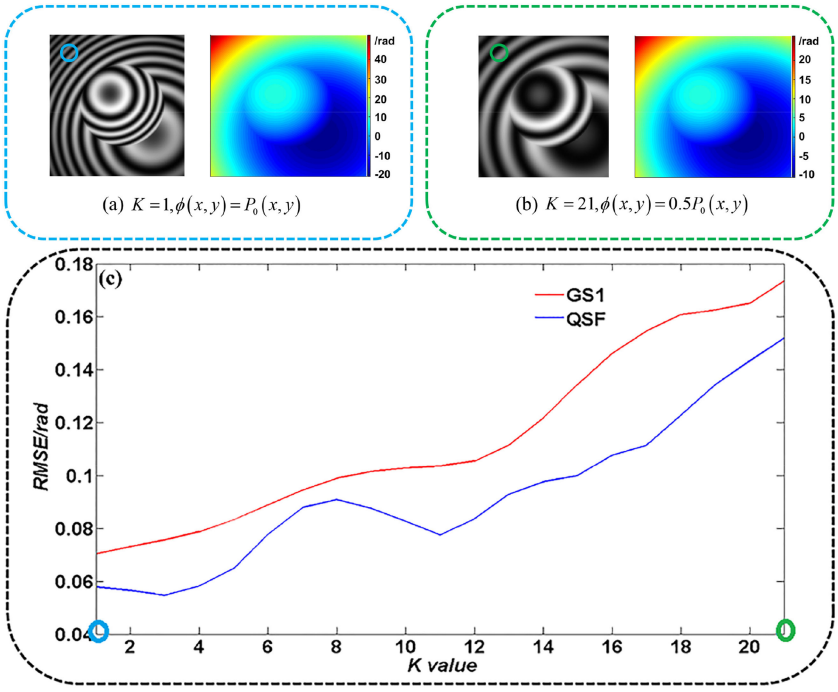

Fig. 4. (a)-(b) The interferograms and reference phases corresponding to the dense fringes and sparse fringes used in Fig. 4(c), respectively; (c) the variation of RMSEs with different K values, in which $A(x, y) = 50exp[-0.1(x^2 + y^2)] + 50$, $B(x, y) = 50exp[-0.1(x^2 + y^2)]$.

In the above simulation, we set $A(x, y) = 50exp[-0.05(x^2 + y^2)] + 50$ and $B(x, y) = 50exp[-0.05(x^2 + y^2)]$ with $\Delta x = \Delta y = 0.01$, then perform the normalization:

$$A(x, y)_{normalized} = \frac{A(x, y) - \bar{A}(x, y)}{A(x, y)} \tag{17a}$$

$$B(x, y)_{normalized} = \frac{B(x, y) - \bar{B}(x, y)}{B(x, y)} \tag{17b}$$

In order to evaluate the simulation results, we introduce two parameters of root mean square error (*RMSE*) and root mean square (*RMS*) to represent the quality of phase retrieval and the spatial variation of a given function, respectively:

$$RMSE_{\phi(x,y)} = \sqrt{\frac{\sum_{x,y}[\phi(x, y) - \phi_0(x, y)]^2}{N}} \tag{18a}$$

$$RMS_{B(x,y)} = \sqrt{\frac{\sum_{x,y}\left[\frac{B(x,y)-\bar{B}(x,y)}{\bar{B}(x,y)}\right]^2}{N}} \tag{18b}$$

Where $\phi_0(x, y)$ represents the ground truth of the phase distribution and $\bar{B}(x, y)$ denotes the spatial average of $B(x, y)$, N denotes the total pixels' number. Clearly, by using a direct-subtracted interferogram, the accuracy of phase retrieval with GS algorithm will become worse ($RMSE_{\phi(x,y)}$= 0.079rad in GS1 and $RMSE_{\phi(x,y)}$= 0.177rad in GS2). And from Figs. 2(b1)-2(b3) and Figs. 2(c1)-2(c3), we can see that the larger spatial variation in the obtained modulation amplitude, the more serious phase distortion.

Furthermore, we present the accuracy variation of phase retrieval with the phase shift and noise level. In Fig. 3(a), the interferograms are corrupted by the random noise with signal noise ratio

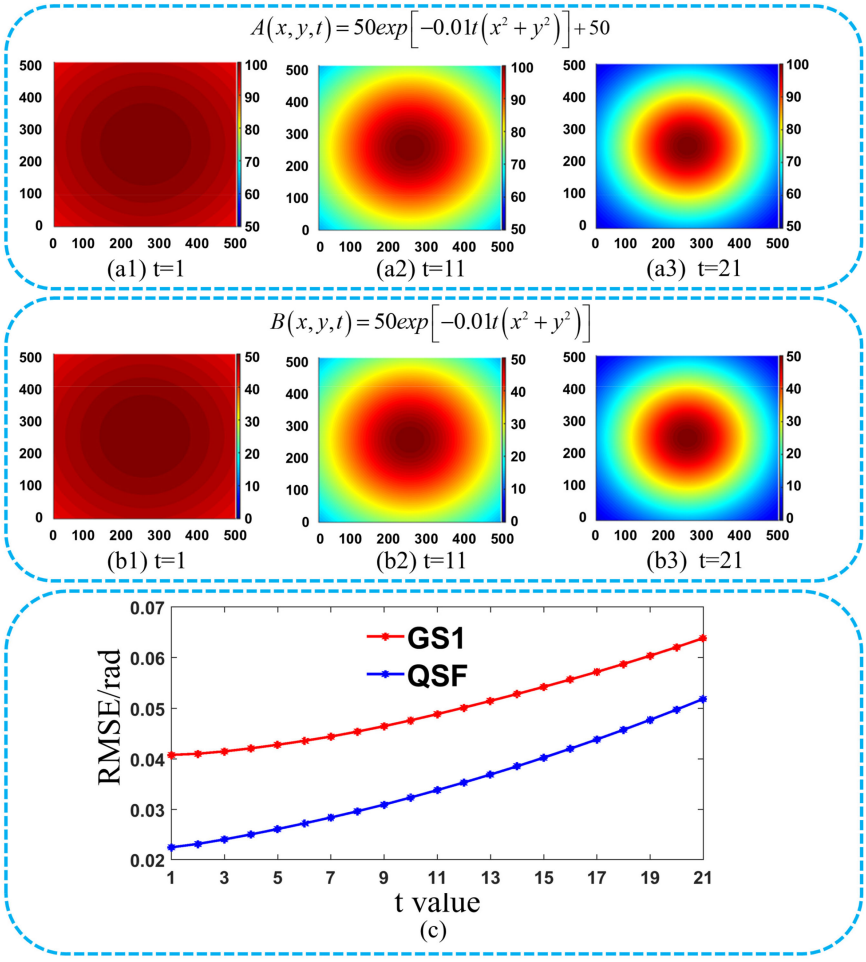

Fig. 5. The variation of phase retrieval with the nonuniformity of illumination by using the GS1 and QSF algorithms, respectively. (a1-a3) the distribution variation of $A(x, y, t) = 50exp[-0.01t(x^2 + y^2)] + 50$ with the time; (b1-b3) the distribution variation of $B(x, y, t) = 50exp[-0.01t(x^2 + y^2)]$ with the time; (c) the variation of phase error with the time.

(SNR) of 45dB and the phase shifts are changed from 0.3rad to 2.8rad; and in Fig. (3b), the phase shift is a constant of 1.5rad and the SNR of 2-frame interferograms are changed from 30dB to 50dB. Clearly, this result demonstrates good performance of the proposed QSF algorithm.

As we know, another important property of PSI method is good accuracy stability under different fringe density. Using the proposed QSF algorithm, Fig. 4 shows the RMSEs of phase retrieval under different fringe density, in which P_0 is chosen as a reference phase model, and the function $\phi_K = [1 - 0.025(K - 1)]P_0$ is used to generate interference patterns with different fringe density. The larger K value, the sparser fringe patterns.

Clearly, along with K increasing, the accuracy of phase retrieval with the GS1 and QSF algorithms is decreased due to the phase distortion increasing. Meanwhile, it is found that in QSF algorithm, when the fringe pattern becomes sparse, the accuracy advantage with a directly subtracted interferogram becomes obvious.

Furthermore, in QSF algorithm, it is assumed that $B(x, y)$ is a slow variation signal, so we need to examine the accuracy of phase retrieval with the uniformity of illumination. As shown in Fig. 5, we set $A(x, y, t) = 50exp[-0.01t(x^2 + y^2)] + 50$, $B(x, y, t) = 50exp[-0.01t(x^2 + y^2)]$. It is found when $t = 21$, $A(x, y)$ and $B(x, y)$ are respectively reduced to about 50% and 10% of the spatial maximum value near the edge of interferogram($A(x, y) > B(x, y)$ must be satisfied). That is to say, although the

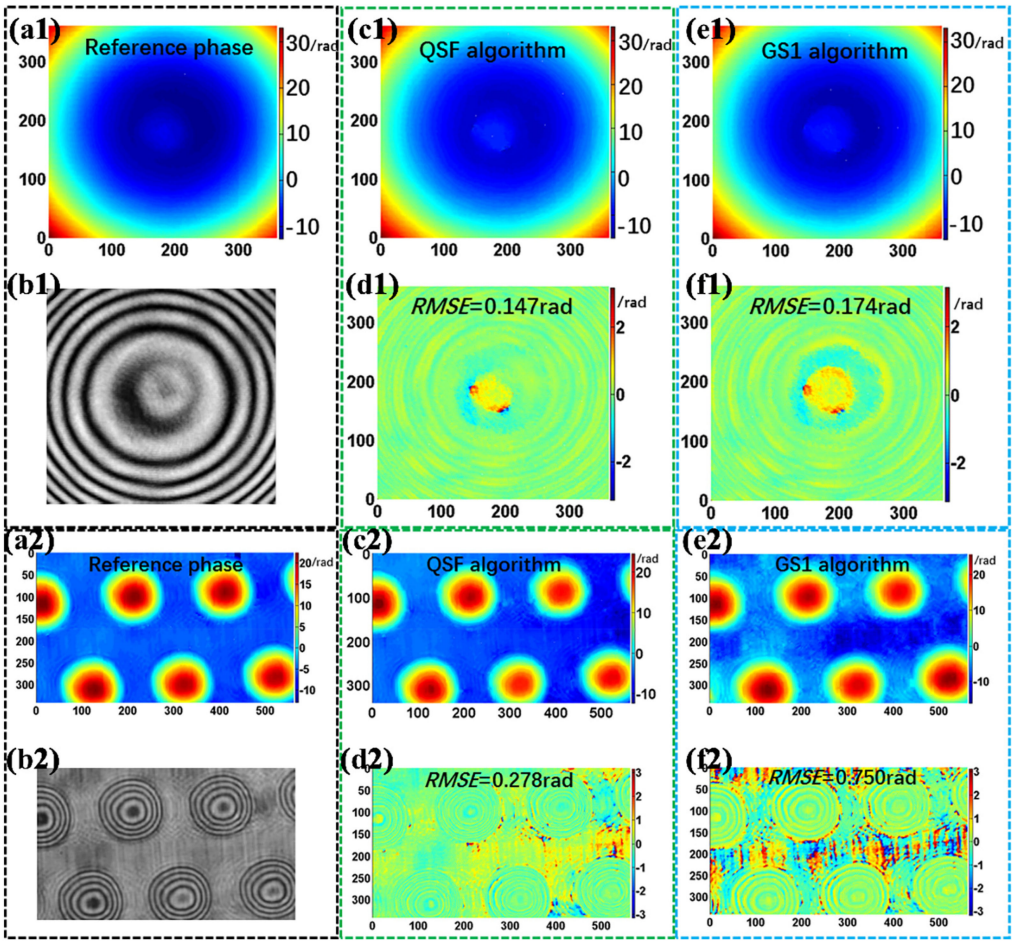

Fig. 6. The quantitative evaluation of phase retrieval with the QSF and GS1 algorithms, respectively. The reference phases and interferograms used (a1) (b1) in the first group; (a2) (b2) in the second group; (c1) (c2) the phase distributions of (b1) (b2) obtained by the QSF algorithm, respectively; (d1) (d2) the phase errors between (b1) (b2) and (c1) (c2), respectively; (e1) (e2) the phase distributions of (b1) (b2) obtained by GS1 algorithm, respectively; (f1) (f2) the phase errors between (a1) (a2) and (e1) (e2), respectively.

accuracy of phase retrieval is decreased with the nonuniformity increasing of illumination, the QSF algorithm still works well under a reasonable illumination.

4. Experimental Research

In this section, we will verify the feasibility of the proposed QSF algorithm by the experimental research. A He-Ne frequency stabilized laser with wavelength of 632.8nm is employed as the illumination source, a holographic microscopy system is built based on the Mach-Zehnder interferometer. A HeLa cell is used as the sample. In the first group, the circular fringes with the aberration phase in the interferogram are captured, and the reference phase is calculated from 150-frame temporal phase-shifting interferograms by using the advanced least square iterative algorithm (AIA) [15] method. Subsequently, the 1st and 25th interferograms are chosen to perform phase retrieval, the obtained results with the QSF and GS1 algorithms are shown in Figs. 6(a1)-6(f1), respectively. In the second group, in order to remove the phase aberration, the interferometric system is modified as a telecentric one [44]–[45], in which the fringe number is reduced. In this

case, we can estimate the phase aberration induced by the sample. Actually, the fringe number decreasing will lead to the accuracy decreasing of background intensity estimation in 2-step PSI, and the phase distortion induced by the spatial filtering will become obvious when the fringe becomes sparse. Consequently, the proposed QSF algorithm will reveal obvious advantage under the suppression of phase distortion. As shown in Figs. 6(a2)-6(f2), after the unwrapping operation [46], in GS1 algorithm, a serious cloud-like phase distortion appears (Fig. 6(e2)) while the phase retrieved by the proposed QSF algorithm reveals high accuracy (Fig. 6(c2)) (The Matlab codes and the experimental data are shared at [47].

5. Conclusion

In this study, we propose a new 2-step PSI solution named as QSF algorithm to perform phase retrieval, in which both interference signal separation and blind phase shift estimation can be realize by using the quadratic spatial filtering (QSF) operation of interferogram. Specially, it is found that the phase distortion induced by the spatial filtering operation, a main error source in the existed 2-step PSI algorithm, can be effectively released by using the QSF algorithm. Moreover, the obtained results demonstrate that the blind phase shift estimation is not related to the statistical property of phase distribution, so the needed fringe number is reduced. Both the simulation and experimental results demonstrate excellent performance of the proposed QSF algorithm, and this will provide a good solution for phase retrieval in 2-step PSI.

References

[1] D. Malacara, M. Servín, and Z. Malacara, *Interferogram Analysis for Optical Testing*, 2nd ed. Boca Raton, FL, USA: CRC Press, 2005.
[2] G. Popescu, *Quantitative Phase Imaging of Cells and Tissues*. New York, NY, USA: Mcgraw-Hill, 2011.
[3] D. Paganin and K. A. Nugent, "Noninterferometric phase imaging with partially coherent light," *Phys. Rev. Lett.*, vol. 80, no. 12, pp. 2586–2589, Mar. 1998.
[4] L. Tian and L. Waller, "Quantitative differential phase contrast imaging in an LED array microscope," *Opt. Exp.*, vol. 23, no. 9, pp. 11394–11403, May 2015.
[5] G. Zheng, R. Horstmeyer, and C. Yang, "Wide-field, high-resolution Fourier ptychographic microscopy," *Nat. Photonics*, vol. 7, no. 9, pp. 739–745, Sep. 2013.
[6] J. R. Fienup, "Phase retrieval algorithms: A comparison," *Appl. Opt.*, vol. 21, no. 15, pp. 2758–2769, Aug. 1982.
[7] T. Zhang and I. Yamaguchi, "Three-dimensional microscopy with phase-shifting digital holography," *Opt. Lett.*, vol. 23, no. 15, pp. 1221–1223, Aug. 1998.
[8] Z. Wang *et al.*, "Spatial light interference microscopy (SLIM)," *Opt. Exp.*, vol. 19, no. 2, pp. 1016–1026, Jan. 2011.
[9] S. K. Debnath and Y. Park, "Real-time quantitative phase imaging with a spatial phase-shifting algorithm," *Opt. Lett.*, vol. 36, no. 23, pp. 4677–4679, Dec. 2011.
[10] T. Kakue *et al.*, "High-speed phase imaging by parallel phase-shifting digital holography," *Opt. Lett.*, vol. 36, no. 21, pp. 4131–4133, Nov. 2011.
[11] N. T. Shaked, Y. Zhu, M. T. Rinehart, and A. Wax, "Two-step-only phase-shifting interferometry with optimized detector bandwidth for microscopy of live cells," *Opt. Exp.*, vol. 17, no. 18, pp. 15585–15591, Aug. 2009.
[12] R. Zhu, B. Li, R. Zhu, Y. He, and J. Li, "Phase extraction from two phase-shifting fringe patterns using spatial-temporal fringes method," *Opt. Exp.*, vol. 24, no. 7, pp. 6814–6824, Apr. 2016.
[13] P. J. de Groot, "Vibration in phase-shifting interferometry," *J. Opt. Soc. Am. A.*, vol. 12, no. 2, pp. 354–365, Feb. 1995.
[14] J. Schwider *et al.*, "Digital wave-front measuring interferometry: Some systematic error sources," *Appl. Opt.*, vol. 22, no. 21, pp. 3421–3432, Nov. 1983.
[15] Z. Wang and B. Han, "Advanced iterative algorithm for phase extraction of randomly phase-shifted interferograms," *Opt. Lett.*, vol. 29, no. 14, pp. 1671–1673, Jul. 2004.
[16] J. Vargas, J. A. Quiroga, and T. Belenguer, "Phase-shifting interferometry based on principal component analysis," *Opt. Lett.*, vol. 36, no. 8, pp. 1326–1328, Apr. 2011.
[17] Y. Wang, B. Li, L. Zhong, J. Tian, and X. Lu, "Spatial dual-orthogonal (SDO) phase-shifting algorithm by pre-recomposing the interference fringe," *Opt. Exp.*, vol. 25, no. 12, pp. 17446–17456, Jun. 2017.
[18] Q. Hao, Q. Zhu, and Y. Hu, "Random phase-shifting interferometry without accurately controlling or calibrating the phase shifts," *Opt. Lett.*, vol. 34, no. 8, pp. 1288–1290, Apr. 2009.
[19] Y. Wang, X. Lu, Y. Liu, J. Tian, and L. Zhong, "Self-calibration phase-shifting algorithm with interferograms containing very few fringes based on fourier domain estimation," *Opt. Exp.*, vol. 25, no. 24, pp. 29971–29982, Nov. 2017.
[20] Q. Weijuan, Y. Yingjie, C. O. Choo, and A. Asundi, "Digital holographic microscopy with physical phase compensation," *Opt. Lett.*, vol. 34, no. 8, pp. 1276–1278, Apr. 2009.
[21] M. Takeda, H. Ina, and S. Kobayashi, "Fourier-transform method of fringe-pattern analysis for computer-based topography and interferometry," *J. Opt. Soc. Am.*, vol. 72, no. 1, pp. 156–160, Jan. 1982.

[22] Y. Wang *et al.*, "General spatial phase-shifting interferometry by optimizing the signal retrieving function," *Opt. Exp.*, vol. 25, no. 7, pp. 7170–7180, Apr. 2017.
[23] M. Servín, J. A. Quiroga, and J. M. Padilla, *Fringe Pattern Analysis For Optical Metrology: Theory, Algorithms, and Applications*. Weinheim, Germany, Wiley-VCH, 2014.
[24] T. M. Kreis and W. P. Jueptner, "Fourier transform evaluation of interference patterns: Demodulation and sign ambiguity," in *Proc. SPIE*, Bellingham, WA, USA, vol. 1553, pp. 263–273, 1992.
[25] J. Vargas, J. A. Quiroga, T. Belenguer, M. Servín, and J. C. Estrada, "Two-step self-tuning phase-shifting interferometry," *Opt. Exp.*, vol. 19, no. 2, pp. 638–648, Jan. 2011.
[26] J. Vargas, J. A. Quiroga, C. O. S. Sorzano, J. C. Estrada, and J. M. Carazo, "Two-step interferometry by a regularized optical flow algorithm," *Opt. Lett.*, vol. 36, no. 17, pp. 3485–3487, Sep. 2011.
[27] J. Vargas, J. A. Quiroga, C. O. S. Sorzano, J. C. Estrada, and J. M. Carazo, "Two-step demodulation based on the gram-schmidt orthonormalization method," *Opt. Lett.*, vol. 37, no. 3, pp. 443–445, Feb. 2012.
[28] J. Deng, H. Wang, F. Zhang, D. Zhang, L. Zhong, and X. Lu, "Two-step phase demodulation algorithm based on the extreme value of interference," *Opt. Lett.*, vol. 37, no. 22, pp. 4669–4671, Nov. 2012.
[29] L. Fengwei *et al.*, "Simultaneous extraction of phase and phase shift from two interferograms using lissajous figure and ellipse fitting technology with hilbert–huang prefiltering," *J. Opt.*, vol. 18, no. 10, 2016, Art. no. 105604.
[30] C. Tian and S. Liu, "Two-frame phase-shifting interferometry for testing optical surfaces," *Opt. Exp.*, vol. 24, no. 16, pp. 18695–18708, Aug. 2016.
[31] C. Tian and S. Liu, "Demodulation of two-shot fringe patterns with random phase shifts by use of orthogonal polynomials and global optimization," *Opt. Exp.*, vol. 24, no. 4, pp. 3202–3215, Feb. 2016.
[32] J. Ma, Z. Wang, and T. Pan, "Two-dimensional continuous wavelet transform algorithm for phase extraction of two-step arbitrarily phase-shifted interferograms," *Opt. Lasers Eng.*, vol. 55, no. apr, pp. 205–211, Apr. 2014.
[33] M. Wielgus, Z. Sunderland, and K. Patorski, "Two-frame tilt-shift error estimation and phase demodulation algorithm," *Opt. Lett.*, vol. 40, no. 15, pp. 3460–3463, Aug. 2015.
[34] C. Tian and S. Liu, "Phase retrieval in two-shot phase-shifting interferometry based on phase shift estimation in a local mask," *Opt. Exp.*, vol. 25, no. 18, pp. 21673–21683, Sep. 2017.
[35] D. O. Hogenboom, C. A. DiMarzio, T. J. Gaudette, A. J. Devaney, and S. C. Lindberg, "Three-dimensional images generated by quadrature interferometry," *Opt. Lett.*, vol. 23, no. 10, pp. 783–785, May 1998.
[36] W. C. Warger and C. A. DiMarzio, "Computational signal-to-noise ratio analysis for optical quadrature microscopy," *Opt. Exp.*, vol. 17, no. 4, pp. 2400–2422, Feb. 2009.
[37] A. Safrani and I. Abdulhalim, "Real-time phase shift interference microscopy," *Opt. Lett.*, vol. 39, no. 17, pp. 5220–5223, Sep. 2014.
[38] P. Sun, L. Zhong, C. Luo, W. Niu, and X. Lu, "Visual measurement of the evaporation process of a sessile droplet by dual-channel simultaneous phase-shifting interferometry," *Sci. Rep.*, vol. 5, 2015, Art. no. 12053.
[39] K. Freischlad and C. L. Koliopoulos, "Fourier description of digital phase-measuring interferometry," *J. Opt. Soc. Am. A.*, vol. 7, no. 4, pp. 542–551, Apr. 1990.
[40] R. C. Gonzalez and R. E. Woods, *Digital Image Processing*, 3rd ed. Englewood Cliffs, NJ, USA: Prentice-Hall, 2007.
[41] J. A. Quiroga, J. A. Gómez-Pedrero, and Á. García-Botella, "Algorithm for fringe pattern normalization," *Opt. Commun.*, vol. 197, no. 1-3, pp. 43–51, Sep. 2001.
[42] K. Pokorski and K. Patorski, "Separation of complex fringe patterns using two-dimensional continuous wavelet transform," *Appl. Opt.*, vol. 51, no. 35, pp. 8433–8439, Dec. 2012.
[43] M. Trusiak and K. Patorski, "Two-shot fringe pattern phase-amplitude demodulation using gram-schmidt orthonormalization with hilbert-huang pre-filtering," *Opt. Exp.*, vol. 23, no. 4, pp. 4672–4690, Feb. 2015.
[44] E. Sánchez-Ortiga, P. Ferraro, M. Martínez-Corral, G. Saavedra, and A. Doblas, "Digital holographic microscopy with pure-optical spherical phase compensation," *J. Opt. Soc. Am. A*, vol. 28, no. 7, pp. 1410–1417, Jul. 2011.
[45] A. Doblas, E. Sánchez-Ortiga, M. Martínez-Corral, G. Saavedra, P. Andrés, and J. Garcia-Sucerquia, "Shift-variant digital holographic microscopy: Inaccuracies in quantitative phase imaging," *Opt. Lett.*, vol. 38, no. 8, pp. 1352–1354, Apr. 2013.
[46] N. Pandey, A. Ghosh, and K. Khare, "Two-dimensional phase unwrapping using the transport of intensity equation," *Appl. Opt.*, vol. 55, no. 9, pp. 2418–2425, Mar. 2016.
[47] [Online]. Available: https://pan.baidu.com/s/17zVMeaMq7xTABJCPQiGBpQ